Electrochimica Acta 244 (2017) 222–229

Contents lists available at ScienceDirect

Electrochimica Acta

journal homepage: www.elsevier.com/locate/electacta

Dual–phase Spinel $MnCo_2O_4$ Nanocrystals with Nitrogen-doped Reduced Graphene Oxide as Potential Catalyst for Hybrid Na–Air Batteries

Yao Kang[a], Da Zou[a], Jianyong Zhang[a], Feng Liang[a,b,*], Katsuro Hayashi[c], He Wang[c], Dongfeng Xue[d], Kunfeng Chen[d], Keegan R. Adair[e], Xueliang Sun[e]

[a] Faculty of Metallurgical and Energy Engineering, Kunming University of Science and Technology, Kunming 650093, China
[b] State Key Laboratory of Complex Nonferrous Metal Resources Clean Utilization, Kunming University of Science and Technology, Kunming 650093, China
[c] Department of Applied Chemistry, Faculty of Engineering, Kyushu University, Fukuoka 819-0395, Japan
[d] State Key Laboratory of Rare Earth Resources Utilization, Chinese Academy of Sciences, Changchun 130022, China
[e] Department of Mechanical and Materials Engineering, University of Western Ontario, London, Ontario N6A 5B9, Canada

ARTICLE INFO

Article history:
Received 4 March 2017
Received in revised form 10 May 2017
Accepted 15 May 2017
Available online 18 May 2017

Keywords:
Dual-phase spinel $MnCo_2O_4$
Electrocatalyst
Na-air battery
Aqueous electrolyte
Overpotential

ABSTRACT

The electrochemical performance of Na–air batteries have a significant dependence on the type of electrocatalyst used for the oxygen reduction reaction (ORR) and oxygen evolution reaction (OER). Herein, a dual-phase spinel $MnCo_2O_4$ with nitrogen-doped reduced graphene oxide hybrid (*dp*-$MnCo_2O_4$/N-rGO) employed in a hybrid Na-air battery system was demonstrated simultaneous electrocatalytic characteristic toward both ORR and OER, which showed comparable ORR and superior OER catalytic performance over commercial Pt/C. The fabricated dual-phase cobalt manganese spinel nanoparticles, the introduced dopants (nitrogen atoms), and the electrical and chemical coupling between the oxide nanoparticles and nanocarbon backbones significantly contribute to the high catalytic performance of *dp*-$MnCo_2O_4$/N-rGO. The proposed catalyst exhibited a slightly higher discharge voltage of 2.75 V and lower charge voltage of 3.14 V compared to that of a commercial Pt/C (2.73 and 3.35 V, respectively). The hybrid battery showed a low overpotential of 0.39 V and improved round-trip energy efficiency. The battery exhibited excellent discharge stability and no significant degradation was observed during the 25 cycles due to the moderate particle size of *dp*-$MnCo_2O_4$ and large active N-doped surface area. Therefore, *dp*-$MnCo_2O_4$/N-rGO could be a promising bifunctional catalyst for enhancing the electrochemical performance of hybrid Na-air batteries.

© 2017 Elsevier Ltd. All rights reserved.

1. Introduction

The growing interest in electric vehicles and portable electronics has increased the demand for smaller and lighter batteries. Li-ion batteries have been successfully used in portable electronics due to their lightweight design, flexibility, stability, and safety [1–4]. Previously, researchers have explored Li-ion batteries for applications in electric vehicles and energy storage due to their superior capacity and energy densities compared to other battery technologies, such as nickel–cadmium or lead-acid and so on [4–11]. However, the future application of Li-ion batteries is limited due to the insufficient cell voltage and capacity of materials for cathodes and anodes [4,12].

Li-air batteries have been regarded as next generation energy storage devices and investigated for many years due to their extremely high theoretical capacity [13–15]. However, these batteries exhibit poor cyclic stability, large overpotentials, and limited discharge efficiency as well as expensive and impractical [16–21]. The overpotential of lithium-air batteries can be decreased using cathodes that consist of nanoscale amorphous lithia confined in cobalt oxide to enable charge/discharge between solid $Li_2O/Li_2O_2/LiO_2$ without gas evolution; nevertheless, these batteries face manufacturing problems [20]. In this regard, Na-air batteries have gained much attention as next generation power storage because of their high theoretical specific density and capacity, which are several times higher than those of conventional Li-ion batteries [21–23]. Moreover, sodium is more abundant on

* Corresponding author. Xuefu Road 253, Kunming City, Yunnan Province, P.R. China, 650093. Tel.: +86 871 6510720; fax: +86 871 6510720.
E-mail address: liangfeng@kmust.edu.cn (F. Liang).

http://dx.doi.org/10.1016/j.electacta.2017.05.100
0013-4686/© 2017 Elsevier Ltd. All rights reserved.

the earth than lithium, thereby enabling the sustainable development of modern industries [22–25].

Generally, Na-air batteries are classified based on electrolytes used in the system; these batteries could either be non-aqueous or hybrid, whose reactions are as follows:

$$\text{Non-aqueous: Na+ } O_2 \leftrightarrow NaO_2 \quad (1)$$

$$Na + 1/2O_2 \leftrightarrow 1/2Na_2O_2 \quad (2)$$

$$\text{Hybrid: } Na + 1/4O_2 + 1/2H_2O \leftrightarrow NaOH \quad (3)$$

Non-aqueous Na-air batteries present significant limitations in terms of practical energy and capacity because of the insolubility of the discharge products (e.g., Na_2O and Na_2O_2) in the organic electrolyte which results in insoluble product growth and clogging of the porous air electrode [23–29]. To solve this, scholars have developed hybrid Na-air batteries by using aqueous electrolyte (NaOH) to solve the blocking of insoluble discharge products [21–23]. In addition, hybrid Na-air batteries possess a higher standard voltage of 3.11 V and specific capacity of 838 mAh g^{-1} and lower overpotential than non-aqueous Na-air batteries [21–30]. Despite these advantages, the oxygen reduction and evolution at the cathode of Na-air batteries are slow, hence, Na-air batteries usually require noble metal catalysts, such as Pt or its alloys, to retain high discharge voltage and low charge voltage [31,32]. For instance, Kim *et al.* investigated the charge–discharge properties of batteries with Pt/C-coated carbon paper as an air electrode [31]. The hybrid Na-air battery exhibited higher voltage efficiency (84.3%) than those with Vulcan XC72R-coated carbon paper (78%) and uncoated carbon paper (72.4%). Although Pt/C shows desirable ORR catalytic activity, its large-scale application in reversible air electrodes is impeded by its high cost, scarcity, and unsatisfactory OER activity [18]. Therefore, future works should develop highly effective bifunctional catalysts for ORR and OER.

Carbon-based materials have been proposed as an effective catalyst for ORR in non-aqueous Na-air batteries [33,34]. The diverse structures and morphologies of these carbonaceous materials enable the optimization of oxygen/electrolyte diffusion and electron transport. Liu *et al.* first proposed graphene nanosheets (GNSs) as an effective catalyst in non-aqueous Na-air batteries in 2013; GNSs exhibited a higher discharge capacity of 9268 mAh g^{-1} at discharge current density of 200 mA g^{-1} [33]. Moreover, N-doped carbon materials have gained increased research attention due to their stronger electrocatalytic characteristics as cathode materials compared to pure carbon materials. Sun *et al.* applied N-GNSs as a catalyst, which demonstrated a discharge capacity that is two times higher than its counterpart (GNSs) for non-aqueous Na-air batteries. The active sites introduced by nitrogen doping were analyzed to explain the superior electrocatalytic activity of N-GNSs [35,36], because the dopants (nitrogen atoms) provide numerous available active sites, resulting in enhanced catalytic activity. Scholars have also investigated carbon nanotubes (CNTs), N-doped CNTs, and other carbon materials, which all exhibited high performances, as effective catalysts for Na-air batteries. In addition, graphitic nanoshell/mesoporous carbon hybrids (GNS/MC) have been proposed as highly efficient and stable bifunctional oxygen electrocatalysts for rechargeable aqueous Na-air batteries [37]. Although GNS/MC showed a low overpotential of around 0.12 V, the synthesis methods employed are too complicated for large-scale production and the catalyst still exhibited undesirable performance for ORR.

Catalysts based on nonprecious metal oxides have been widely investigated to enhance the electrochemical performance of hybrid Na-air batteries; these catalysts exhibit high catalytic performance and low costs. Liang *et al.* first used Mn_3O_4/C as an effective catalyst for hybrid Na-air batteries, which possessed a discharge voltage of 2.6 V at a current density of 1 mA cm^{-2} [22]. Another work on hybrid Na-air batteries used $Co_3(PO_4)_2$, which exhibited satisfactory ORR catalytic performance [32]. However, $Co_3(PO_4)_2$ displayed a high charge voltage, resulting in a large overpotential of 0.59 V. Generally, most metal oxides possess lower electrical conductivity than carbon-based materials; a defining characteristic that may limit electron transport on catalytically active sites. This issue becomes prominent in high-current density regions, where large amounts of electrons flood into and out of the reaction sites on the electrode surface during ORR and OER [38]. Therefore, developing bifunctional catalysts to efficiently catalyze both ORR and OER in hybrid Na-air batteries remains highly desirable yet challenging.

In this paper, we present dual-phase spinel $MnCo_2O_4$ with nitrogen-doped reduced graphene oxide hybrids for ORR and OER. Compared with commercial Pt/C, the fabricated Na-air battery displayed a relatively low overpotential of 0.39 V. The developed battery also exhibited excellent discharge stability. Moreover, no significant degradation was observed during the 25 cycles. Therefore, dual-phase spinel $MnCo_2O_4$ with nitrogen-doped reduced graphene oxide hybrids can be a potential catalyst for hybrid Na-air batteries.

2. Experimental

2.1. Preparation of air catalytic electrode

Synthesis of $MnCo_2O_4$ nanocrystals: Briefly, 698 mg of Co $(NO_3)_2{\cdot}6H_2O$ and 344 mg of $Mn(NO_3)_2{\cdot}6H_2O$ were dissolved in 55 mL of deionized (DI) water under gentle magnetic stirring to obtain a homogeneous solution. Subsequently, 288 mg of NaOH was dissolved in 5 mL of DI water; the solution was added dropwise into the reaction mixture under vigorous stirring for 30 min. The reaction mixture was then transferred into a 65 mL Teflon-lined stainless steel autoclave. The hydrothermal reaction was carried out at 160 °C for 10 h. The products were collected, washed four times with water and ethanol mixture (volume ratio 1:1), and dried at 40 °C. The obtained powder was calcined in air at 400 °C for 1 h.

Synthesis of *dp*-$MnCo_2O_4$/N-rGO: Graphene oxide (GO) powders were prepared according to typical Hummer's method [39]. A 0.1 mg/mL GO solution was prepared by diluting 1 wt % GO stock solution. The pH of the GO solution was adjusted to 8 by adding aqueous ammonia. The GO solution was added with an appropriate amount of the calcined spinel $MnCo_2O_4$ to obtain 4:1 weight ratio of $MnCo_2O_4$ to GO. The solution was then added with urea with weight 200 times higher than that of GO. The solution was sonicated for 1 h to obtain a homogeneous mixture, which was transferred to a Teflon-lined stainless steel autoclave. Hydrothermal treatment was carried out at 170 °C for 12 h. The resulting hybrid catalyst was collected by centrifugation, washed four times with water and ethanol mixture, and dried at 40 °C.

2.2. Assembly of the Na-air battery

Fig. 1a shows the schematic of the fabricated hybrid Na-air battery, which consists of a sodium metal anode, 1 M $NaClO_4$ in EC/DMC (1:1) with 1 vol% FEC as anolyte, a solid conductor with $Na_3Zr_2Si_2PO_{12}$ (ionic conductivity of 1.3×10^{-3} S cm^{-1} at 25 °C) [22], 1 M NaOH as catholyte, and a porous air electrode containing *dp*-$MnCo_2O_4$/N-rGO hybrid as catalyst. During discharge, oxygen from the air diffuses into the catalytic sites, is reduced on the catholyte/catalyst (*dp*-$MnCo_2O_4$/N-rGO)/air three-phase interface,

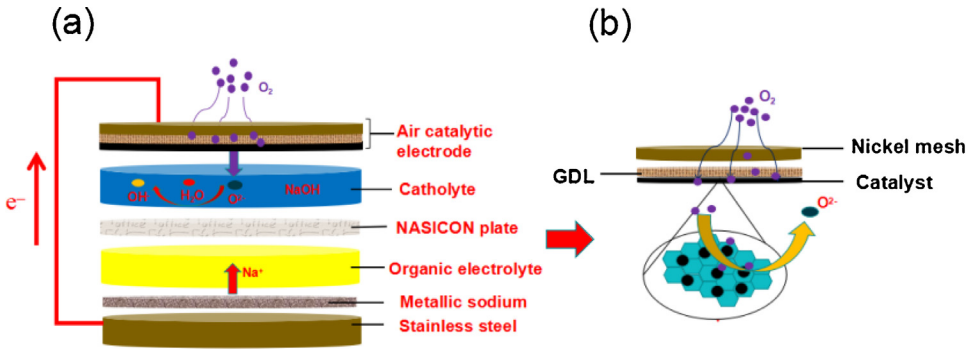

Fig. 1. (a) Schematic of a typical hybrid Na-air battery. (b) ORR on the *dp*-$MnCo_2O_4$/N-rGO surface.

and combines with H_2O and electrons in the cathode to form OH^-. In the organic electrolyte, metallic sodium is oxidized into Na^+ and diffuses through organic electrolyte and NASICON solid separator into the catholyte. Fig. 1b depicts the detailed ORR process on the active sites on the *dp*-$MnCo_2O_4$/N-rGO surface. During discharge, oxygen from the air diffuses into the catalytic sites and is reduced on the catholyte/*dp*-$MnCo_2O_4$/N-rGO/air three-phase interface. The electronic state of the Mn^{4+}/Mn^{3+} redox couples was tailored by introducing nanocarbon materials to establish covalent interfacial Mn–O–C interactions (Mn–N–C interactions for nitrogen doped sites), where electron sharing between C and O reduces the electron cloud density around Mn [38]. Correspondingly, the molecular orbital sharing between $MnCo_2O_4$ and nanocarbon shifts the Mn^{4+}/Mn^{3+} redox couple towards the Mn^{3+} state, thereby improving ORR activities.

Five different catalyst inks were prepared by sonicating 15 mg of *dp*-$MnCo_2O_4$/N-rGO, Pt/C 40% (JJ040, China), N-rGO, dp-$MnCo_2O_4$, and carbon black (EBORY, China) in 2 mL of ethanol with a drop of PTFE as binder. N-rGO was prepared by a typical method [39]. The catalyst inks were then dropped onto the gas diffusion layer (GDL), and air electrodes were obtained by pressing (8 MPa) the catalyst layer onto the nickel mesh. The GDL was prepared by a typical method [40]. The catalyst loading and binder content in the air electrodes were 1 mg cm^{-2} and 20 wt %, respectively. In the hybrid Na-air battery, *dp*-$MnCo_2O_4$/N-rGO, 40 wt % Pt/C, N-rGO, dp-$MnCo_2O_4$, and carbon black were used as catalysts. The assembled Na-air battery was exposed to atmospheric air and connected to the testing station. A LAND cell tester (CT2001A, Wuhan LAND electronics) was used for charge and discharge tests. The electrochemical performance of the hybrid Na-air battery was tested at 25 °C under a relative humidity (R_H) of 70%.

2.3. Material Characterization

X-ray diffraction (XRD) data were collected with an X-ray diffractometer (MiniFlex 600, Japan) equipped with Cu*Kα* radiation from 10° to 90° at a scan rate of 0.02° s^{-1}. Morphology characterizations were performed through transmission electron microscopy (TEM) analysis (JEOL 2010F, America) at 200 keV. X-ray

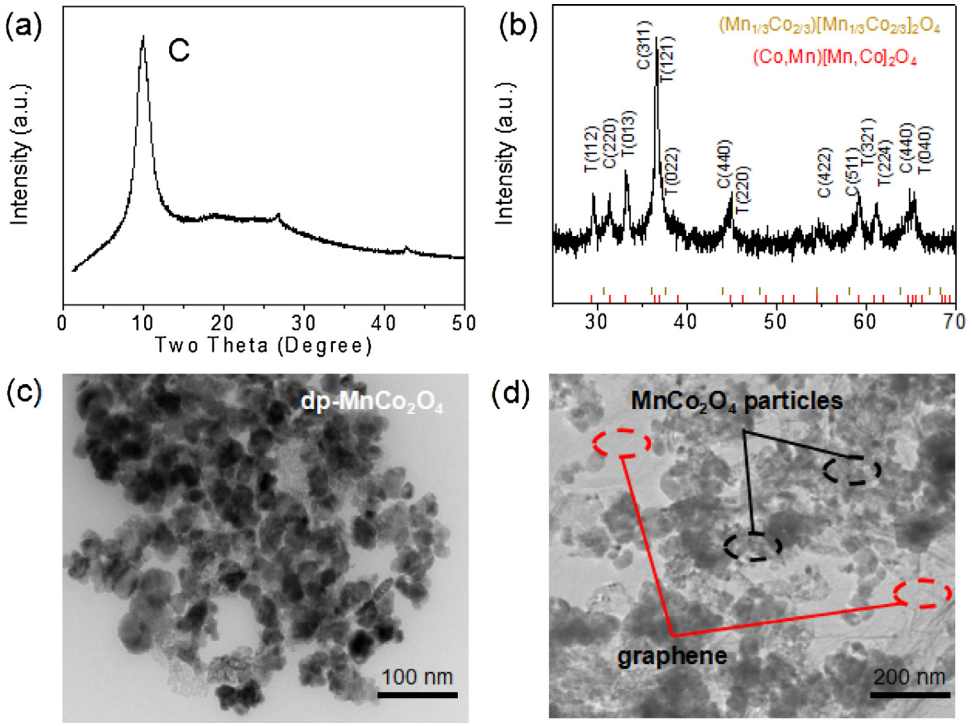

Fig. 2. XRD pattern of (a) graphene oxide and (b) *dp*-$MnCo_2O_4$ nanocrystal *dp*-$MnCo_2O_4$ nanocrystal; and TEM image of (c) *dp*-$MnCo_2O_4$ nanocrystal and (d) *dp*-$MnCo_2O_4$/N-rGO catalysts.

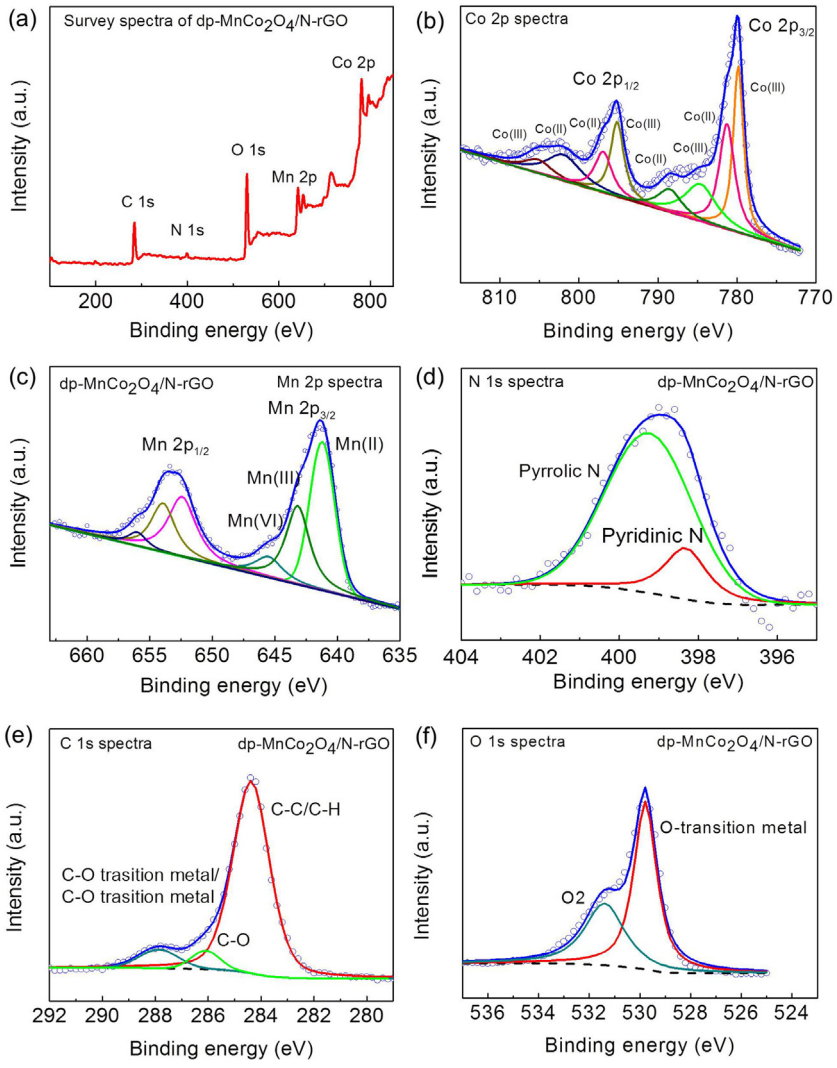

Fig. 3. X-ray photoelectron spectra (a–f) of the Co 2p, Mn 2p, C 1s, N 1s, and O 1s peaks of *dp*-$MnCo_2O_4$/N-rGO, respectively.

photoelectron spectroscopy (XPS) data were collected using a scanning XPS microprobe system (PHI5000 Versaprobe-II, Japan).

3. Results and discussion

Fig. 2a shows the powder XRD pattern of GO. A strong and sharp peak was found at $2\theta = 11^\circ$ in the sample; this peak corresponds to the characteristic diffraction peak of GO powder. Fig. 2b shows the XRD pattern of *dp*-$MnCo_2O_4$, which consists of cubic $(Mn_{1/3}Co_{2/3})[Mn_{1/3}Co_{2/3}]_2O_4$ and tetragonal (Co, Mn)[Mn, Co]$_2O_4$; obvious peak splitting was detected in the powder XRD pattern of the calcined $MnCo_2O_4$. These two sets of diffraction reflections are indexed as cubic $(Mn_{1/3}Co_{2/3})$-$[Mn_{1/3}Co_{2/3}]_2O_4$ phase and the less commonly observed tetragonal (Co, Mn)[Mn, Co]$_2O_4$ phase. The TEM image shows that the particle size of $MnCo_2O_4$ nanocrystals is within 30–60 nm (Fig. 2c), which is slightly larger than the size of particles obtained from two-step methods or one-pot synthesis (average size < 10 nm) [41–44]. This moderate particle size might be advantageous for long-term performance of the catalysts. Fig. 2d shows the TEM image of *dp*-$MnCo_2O_4$/N-rGO hybrid catalysts; dark nanoparticles were clearly observed on the N-GO surface, indicating the successful preparation of the *dp*-$MnCo_2O_4$/N-rGO catalyst.

As shown in Fig. 3, the chemical composition of *dp*-$MnCo_2O_4$/N-rGO was evaluated by XPS analysis. The full XPS spectrum reveals that the as-prepared *dp*-$MnCo_2O_4$/N-rGO hybrid consists of Co, Mn, C, N, and O, indicating that N atoms were successfully doped into the materials. First, the high-resolution spectrum of Co 2p exhibits two doublets due to spin-orbit interaction; these 781 and 798 eV doublets belong to Co $2p_{3/2}$ and Co $2p_{1/2}$ (Fig. 3a). This positive peak shift is also pronounced for Mn cations; the Mn $2p_{3/2}$ core-level spectra show the position at 653 eV, whereas the Mn $2p_{1/2}$ core-level spectra present a peak that down shifted to 642 eV. The Co/Mn ratio on the *dp*-$MnCo_2O_4$/N-rGO surface is lower than the stoichiometric ratio of the bulk oxide, implying preferential accumulation of Mn species on the catalyst surface. Therefore, the high surface exposure of Mn^{4+}/Mn^{3+} redox couple is favorable toward superior ORR performance. Second, the high-resolution N 1s spectra reveal that the doped N atoms existed in the form of pyridinic-N and pyrrolic-N. The ORR activity of N-doped carbon materials was proposed to be dependent on the contents of pyridinic-N and pyrrolic-N, which determine the onset potential for ORR [45]. Therefore, the materials were predicted to exhibit excellent catalytic performance toward ORR considering the high content of N in the hybrid. Third, the C 1s peak is observed at 284.3 eV, which is ascribed to the binding energy of C–C and C–H

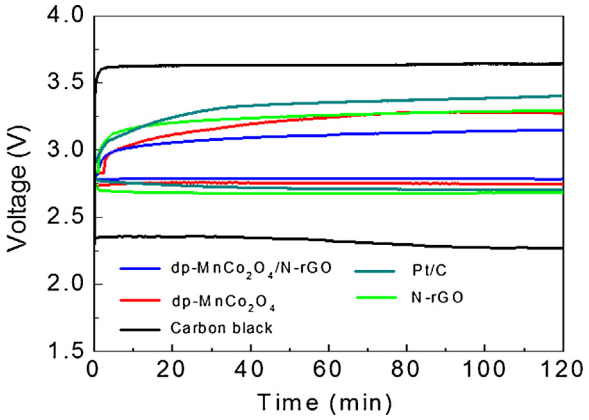

Fig. 4. Charge–discharge profiles of *dp*-$MnCo_2O_4$/N-rGO as catalyst for hybrid Na-air battery in comparison with dp-$MnCo_2O_4$, N-rGO, Pt/C 40 wt% and carbon black at the current density of 0.13 mA cm^{-2}.

bonds (Fig. 3e). The high intensity of the peaks originates from C–O interaction, indicating the presence of a stronger oxidized C environment due to the oxide-nanocarbon interactions. An additional C 1s peak is also observed at 288.3 eV; this peak could be attributed to the formation of C–O–transition metal or C–N–transition metal covalent bonds, which contribute to the strong covalent coupling between the spinel and N-doped graphene. As shown in the Fig. 3d, the N 1s peak at 397 eV is consistent with C–N–transition metal covalent bonds, which significantly contribute to the high performance of *dp*-$MnCo_2O_4$/N-rGO [46]. Furthermore, the high-resolution peak of O 1s at 530 eV is due to metal oxide, and the peak of O 1s at higher binding energy (O2) may be assigned to O = C-N, O = C-OH, and C-O-C [39,46,47].

Fig. 4 shows the discharge–charge curves of the hybrid Na-air battery containing *dp*-$MnCo_2O_4$/N-rGO, N-rGO, dp-$MnCo_2O_4$, 40 wt % Pt/C, and carbon black catalysts at a current density of 0.13 mA cm^{-2} during discharging 2 h. As shown in Fig. 4, the battery with carbon black displayed a discharge voltage of 2.28 V, which corresponds to 73.3% of the standard voltage. Carbon black exhibited low catalytic performance because of its limited specific surface area and few activation sites [31]. Conversely, batteries with other catalysts displayed relatively higher discharge voltage and lower charge voltage. Generally, Pt/C is one of the most effective catalysts for ORR, which has been used by Kim *et al.* [31] to fabricate hybrid Na-air batteries. Therefore, the battery containing 40 wt% Pt/C displayed high discharge voltages of 2.73 V. In addition, high charge voltage of 3.35 V was obtained due to limited OER catalytic performance, which leads to the overpotential of 0.62 V. However, the hybrid Na-air battery with the *dp*-$MnCo_2O_4$/N-rGO catalyst exhibits relatively higher discharge voltage of 2.75 V and lower charge voltage of 3.14 V than that with 40 wt% Pt/C during the discharge process, which leads to a low overpotential of 0.39 V. This result corresponds to a round trip efficiency of 87.6%. Firstly, it is likely that cobalt manganese spinel nanoparticles possess catalytic performance comparable to that of Pt/C due to the intrinsic high activity, high dispersion, and moderate size of the nanoparticles [38]. Double-phase oxides are suitable bifunctional catalysts toward ORR and OER because the alternating valence states of the cations can provide donor–acceptor chemisorption sites for the reversible adsorption/desorption of oxygen [38,43]. Moreover, electronic transfer among cations of different valence states generates relatively low activation energy through the polaron hopping mechanism [38,43]. The dp-$MnCo_2O_4$ also exhibits comparable ORR and superior OER catalytic performances compared to Pt/C. However, it shows lower discharge voltage and higher charge voltage than dp-$MnCo_2O_4$/N-rGO due to limited active sites and low conductivity of dp-$MnCo_2O_4$. Additionally, N-rGO itself can be an effective catalyst toward ORR due to its large specific surface area and diverse carbon structures and morphologies, which enable the possibility to optimize oxygen/electrolyte diffusion and electron transport. Moreover, the dopants (nitrogen atoms) provide numerous available active sites, resulting in the enhanced catalytic activity [39,46]. Similarly, as shown in Fig. 4, N-rGO shows poorer ORR and slightly superior OER catalytic performances compared to Pt/C. However, due to limited active sites [38,39,46], N-rGO displayed relatively poorer ORR and OER performances compared to dp-$MnCo_2O_4$/N-rGO Most importantly, the satisfactory catalytic performance of the catalyst could be mainly attributed to the intimate electrical and chemical coupling

Table 1
Discharge–charge performance of hybrid Na-air batteries with different catalysts.

Catalysts	Discharge voltage (V, plateau)	Charge voltage (V, plateau)	Overpotential[a] (V)	Current densities/NaOH concentration (mol L^{-1})	Ref.
Mn_3O_4/C	2.60	3.51	0.91	1 mA cm^{-2}/1	[22]
Pt/C[1]	2.85	3.38	0.53	0.025 mA cm^{-2}/0.1	[31]
Vulcan XC72R	2.7	3.46	0.76	0.025 mA cm^{-2}/0.1	[31]
Carbon paper	2.6	3.59	0.99	0.025 mA cm^{-2}/0.1	[31]
$Co_3(PO_4)_2$	2.82	3.41	0.59	0.01 mA cm^{-2}/0.1	[32]
Graphitic Nanoshell/Mesoporous Carbon	2.98	3.10	0.12	60 mA g^{-1}/0.1	[37]
Pt/C[2]	3.03	3.21	0.18	60 mA g^{-1}/0.1	[37]
Carambola-shaped VO_2	2.81	3.45	0.64	0.01 mA cm^{-2}/0.1	[48]
Pt/C[3]	2.94	3.55	0.61	0.01 mA cm^{-2}/0.1	[48]
dp-$MnCo_2O_4$/N-rGO	2.75	3.14	0.39	0.13 mA cm^{-2}/1	Present work
Pt/C	2.73	3.35	0.62	0.13 mA cm^{-2}/1	Present work
N-rGO	2.67	3.27	0.60	0.13 mA cm^{-2}/1	Present work
Dp-$MnCo_2O_4$	2.74	3.25	0.49	0.13 mA cm^{-2}/1	Present work
Carbon Black	2.28	3.62	1.34	0.13 mA cm^{-2}/1	Present work

[a] Overpotential gap calculation based on charge–discharge voltage plateau.Pt/C[1], Pt/C[2], and Pt/C[3] represent batteries tested under different conditions (current density and NaOH concentration).

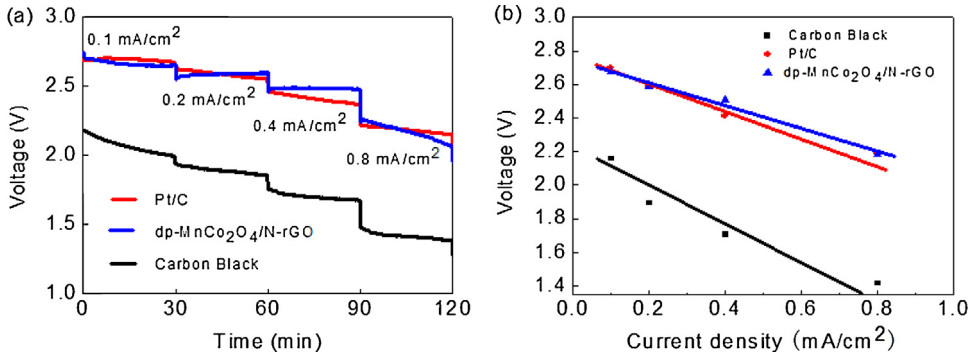

Fig. 5. (a) Discharge voltage profiles of hybrid Na-air batteries with *dp*-$MnCo_2O_4$/N-rGO, Pt/C, and carbon black as catalyst at different current densities. (b) Current density dependence of discharge voltage for batteries with different catalysts. The plots correspond to the measured data, and the solid lines indicate the fitted spectra.

between the oxide nanoparticles and the nanocarbon backbones [38,46]. The integration of metal oxides with nanocarbon materials promotes the formation of a conducting network, which facilitates charge transfer between carbon and the oxide surface [38,46]. However, the discharge voltage obtained in this work is lower than previously reported value possibly because of differences in battery construction and alkaline electrolyte concentration [21]. The discrepancy in discharge voltage could also be due to differences in current densities. Therefore, it is the fabricated dual-phase cobalt manganese spinel nanoparticles, the introduced dopants (nitrogen atoms), and the electrical and chemical coupling between the oxide nanoparticles and nanocarbon backbones that significantly contribute to the high catalytic performance of *dp*-$MnCo_2O_4$/N-rGO.

The comparison of *dp*-$MnCo_2O_4$/N-rGO catalyst with other previous works was summarized in Table 1. As shown in Table 1, the hybrid battery containing *dp*-$MnCo_2O_4$/N-rGO exhibited a lower overpotential of 0.39 V compared with 0.62 V of the battery with Pt/C because of the synergistic effect between *dp*-$MnCo_2O_4$ and N-rGO [38,46][38,46], which contributes to a high roundtrip efficiency of 87.6%. The batteries with *dp*-$MnCo_2O_4$/N-rGO displayed lower discharge voltage than those with GNS/MC and Pt/C due to different battery constructions, concentration of alkaline electrolytes, and current densities; nevertheless, these batteries achieved superior ORR and OER activities compared to the battery with Pt/C under the same test conditions [37]. The catalyst fabricated in this work is the first to achieve a higher discharge voltage than Pt/C in Na-air batteries due to the direct four-electron reduction pathway [38]. This pathway is contributes to the high discharge voltage and low charge voltage of the battery with *dp*-$MnCo_2O_4$/N-rGO, resulting in low overpotential.

Fig. 5 shows the discharge voltage profiles of hybrid Na-air batteries with *dp*-$MnCo_2O_4$/N-rGO, Pt/C, and carbon black as bifunctional catalysts at different current densities. As shown in Fig. 5a, the discharge voltage plateau of the battery with *dp*-$MnCo_2O_4$/N-rGO is lower by 0.20 V than that of Pt/C at 0.10 mA cm^{-2}. The agreement of the results could be due to inefficient contact between the catalyst and NaOH solution. The diverse structures and morphologies of *dp*-$MnCo_2O_4$/N-rGO not only enable the optimization of oxygen/electrolyte diffusion and electron transport in the discharge–charge progress but also limit the number of catalytic sites, resulting in hysteretic catalysis [46]. The dual-phase oxide particles and N-doped graphene formed a complex percolating network for *dp*-$MnCo_2O_4$/N-rGO, which possesses an extremely large interspace and surface area. The incomplete contact between the catalyst and NaOH led to a limited number of functional catalytic sites. The discharge plateau of dp-$MnCo_2O_4$/N-rGO is higher than that of Pt/C at 0.2 mA cm^{-2}, which contributes to the voltage drop of 0.08 V for dp-$MnCo_2O_4$/N-rGO compared to that of 0.11 V for Pt/C. Hence, the increment of the contact between the catalyst and NaOH enhanced the electron transport after long-time work, thereby improving the electrochemical performance [46]. Furthermore, the higher discharge voltage of *dp*-$MnCo_2O_4$/N-rGO compared to that of Pt/C is attributed to the superior ORR catalytic performance and stability of the metal oxide complex [38]. Similarly, the difference in discharge voltage between 0.40 and 0.10 mA cm^{-2} was increased to 0.11 V for *dp*-$MnCo_2O_4$/N-rGO and to 0.29 V for 40 wt% Pt/C. The difference is further increased to 0.49 and 0.51 V at a relatively large current density of 0.8 mA cm^{-2}. The apparent decrease in discharge voltage in Pt/C with increasing current density indicates the relatively inferior catalytic performance of Pt/C; the good conductivity and large catalytic sites of the catalysts promotes the direct reduction of O_2 into OH^-. The decrease in the discharge voltage of the battery with carbon black increased to around 0.74 V, which is larger than those of Pt/C and *dp*-$MnCo_2O_4$/N-rGO.

Fig. 5b shows the current density dependence of the discharge voltage for batteries with different catalysts. The discharge voltage decreased approximately linearly with increasing current density. The slopes of the three catalysts follow the trend of carbon black > Pt/C > *dp*-$MnCo_2O_4$/N-rGO, indicating the superior catalytic performance of *dp*-$MnCo_2O_4$/N-rGO to Pt/C and carbon black. The good electrochemical performance of *dp*-$MnCo_2O_4$/N-rGO highlights the synergistic effect between *dp*-$MnCo_2O_4$ and nitrogen dopants; the abundant functional groups promote uniform nucleation and growth of *dp*-$MnCo_2O_4$ nanoparticles on the N-

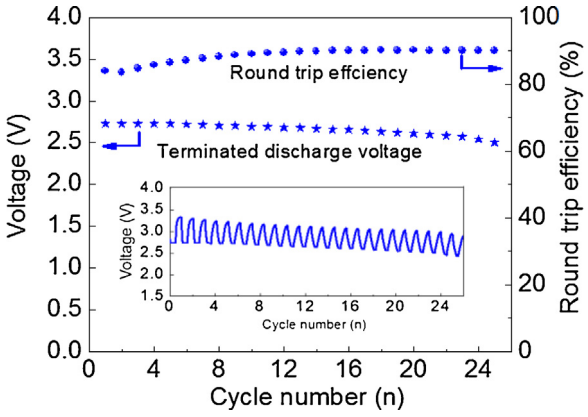

Fig. 6. Cycling performance of the hybrid Na-air battery with *dp*-$MnCo_2O_4$/N-rGO as the catalyst during 25 cycles at a current density of 0.13 mA cm^{-2}.

rGO surface, thereby increasing the number of ORR active sites [39,46].

Fig. 6 shows the cycling performance of the battery with *dp*-$MnCo_2O_4$/N-rGO as an effective bifunctional catalyst. The battery was cycled at a current density of 0.13 mA cm^{-2} for 0.5 h of discharging and charging per cycle. The battery exhibited high discharge efficiency, good durability, and low charge voltage in the first 25 cycles due to the moderate particle size of spinel and the large catalytic site toward O_2 of *dp*-$MnCo_2O_4$/N-rGO. The average discharge plateau is 2.73 V, resulting in a high round trip efficiency. N-doping at the edge of the graphitic layers was believed to be effective for ORR, as it can reduce the energy barrier for oxygen adsorption on adjacent carbon atoms and accelerate the rate limiting first-electron transfer during the ORR [46]. Quantum theory calculation and previous experimental results also suggested that doping of N into graphene planes could induce non-uniform electron distribution and formation of C–N bonds shorter than O–O bonds which facilitate O_2 adsorption and subsequent disassociation/weakening of O = O bonds [39,46]. Furthermore, no decrement was observed in the round trip efficiency during the charge-discharge process, which indicates good cycling performance of this hybrid Na-air battery by using *dp*-$MnCo_2O_4$/N-rGO as catalyst. Due to the limited volume of NaOH solution in this experiment (around 0.2 mL NaOH solution with the concentration of 1 M was utilized as the aqueous catholyte), which resulted the increase of NaOH concentration, and even separation between aqueous electrolyte and catalyst [22]. Therefore, the discharge voltage slightly decreased due to the increasing of NaOH concentration after operated for a long time. Increasing the NaOH concentration enhanced the inter resistance of the battery due to the high solubility of oxygen under alkaline conditions [23].

4. Conclusion

A dual-phase spinel $MnCo_2O_4$ with nitrogen-doped reduced graphene oxide hybrid (*dp*-$MnCo_2O_4$/N-rGO) was prepared by a liquid phase method. The hybrid catalyst was employed in hybrid Na-air batteries and demonstrated simultaneous electro-catalysis toward ORR and OER. The fabricated Na-air battery with the *dp*-$MnCo_2O_4$/N-rGO catalyst displayed slightly higher discharge voltage (2.75 V) and lower charge voltage (3.14 V) than the battery with commercial Pt/C, resulting in a relatively low overpotential of 0.39 V. This paper is the first to report a catalyst that can achieve superior ORR and OER activities compared with Pt/C for hybrid Na-air batteries. The leading preponderance of *dp*-$MnCo_2O_4$/N-rGO could be due to the efficiently established percolating network for electrical conduction, uniform distribution of oxides in graphene catalysts, and an improved covalent coupling between oxide and nitrogen-doped reduced rGO. Therefore, the constructed dual-phase cobalt manganese spinel nanoparticles, the introduced dopants (N atoms), and the intimate electrical and chemical coupling between the oxide nanoparticles and nanocarbon backbones significantly contribute to the high catalytic performance of *dp*-$MnCo_2O_4$/N-rGO. The hybrid Na-air battery also exhibited long-term discharge–charge performance. Moreover, no significant degradation was observed due to the moderate particle size of *dp*-$MnCo_2O_4$ and the large active N-doped surface area. Therefore, *dp*-$MnCo_2O_4$/N-rGO can be a potential candidate for hybrid Na-air batteries and is a promising alternative for Pt/C.

Acknowledgement

This work was financially supported by Open Project of the State Key Laboratory of Rare Earth Resource Utilization (under project No. RERU2016019), the High-level Scientific Research Foundation for the Introduction of Talents in Kunming University of Science and Technology (KKSY201552014), the Scientific Research Foundation of Yunnan Provincial Education Department (KKJA201552027), the Applied Basic Research Programs of Yunnan Provincial Science and Technology Department (KKS0201652014). K. Hayashi also thanks to the financial support from Grant-in-Aid for Scientific Research (KAKENHI No. 26289235 and JP16H6440) of JSPS, and the Elements Strategy Initiative to Form Core Research Center, MEXT, Japan.

References

[1] I. Hadjipaschalis, A. Poullikkas, V. Efthimiou, Overview of current and future energy storage technologies for electric power applications, Renew. Sust. Energ. Rev. 13 (2009) 1513.
[2] H. Chen, T.N. Cong, W. Yang, C.Q. Tan, Y.L. Li, Y.L. Ding, Progress in electrical energy storage system: a critical review, Prog. Nat. Sci. 19 (2009) 291.
[3] A. Manthiram, Materials Challenges and Oportunities of Lithium Ion Batteries, J. Phys. Chem. Lett. 2 (2011) 176.
[4] J. Goodenough, Rechargeable Batteries: Challenges Old and New, J. Solid State Electrochem. 16 (2012) 2019.
[5] N.S. Randhawa, K. Gharami, M. Kumar, Leaching kinetics of spent nickel–cadmium battery in sulphuric acid, Hydrometallurgy. 165 (2015) 191.
[6] J. Zhang, C. Chen, X.Y. Zhang, S.T. Liu, Study on the environmental risk assessment of lead-acid batteries, Pro. Environ. Sci. 31 (2016) 873.
[7] A.B. Ansari, V. Esfahanian, F. Torabi, Discharge, rest and charge simulation of lead-acid batteries using an efficient reduced order model based on proper orthogonal decomposition, Appl. Energ. 173 (2016) 15.
[8] A.A. AbdelHamid, X.F. Yang, J.H. Yang, X.J. Chen, J.Y. Ying, Graphene-wrapped nickel sulfide nanoprisms with improved performance for Li-ion battery anodes and supercapacitors, Nano Energy 26 (2016) 425.
[9] I.D. Seymour, S. Chakraborty, D.S. Middlemiss, D.J. Wales, C.P. Grey, Mapping Structural Changes in Electrode Materials: Application of the Hybrid Eigenvector-Following Density Functional Theory (DFT) Method to Layered $Li_{0.5}MnO_2$, Chem. of Mater. 27 (2015) 5550.
[10] M.M. Sundaram, T. Watcharatharapong, S. Chakraborty, R. Ahuja, S. Duraisamy, P.T. Rao, N. Munichandraiah, Synthesis, and crystal and electronic structure of sodium metal phosphate for use as a hybrid capacitor in non-aqueous electrolyte, Dalton Transactions 44 (2015) 20108.
[11] M. Minakshi, D.R.G. Mitchell, R. Jones, F. Alenazey, T. Watcharatharapong, S. Chakraborty, R. Ahuja, Synthesis, structural and electrochemical properties of sodium nickel phosphate for energy storage devices, Nanoscale 8 (2016) 11291.
[12] D. Deng, Li-ion batteries: basics, progress, and challenges, Energ. Sci. Eng. 3 (2015) 385.
[13] T. Zhang, N. Imanishi, Y. Shimonishi, A. Hirano, Y. Takeda, O. Yamamotoa, N. Sammesb, A novel high energy density rechargeable lithium/air battery, Chem. Commun. 46 (2010) 1661.
[14] H. He, W. Niu, N.M. Asl, J. Salim, R. Chen, Y. Kim, Effects of aqueous electrolytes on the voltage behaviors of rechargeable Li-air batteries, Electrochim. Acta 67 (2012) 87.
[15] P. He, T. Zhang, J. Jiang, H. Zhou, Lithium–Air Batteries with Hybrid Electrolytes, J. Phys. Chem. Lett. 7 (2016) 1267.
[16] J. Lu, J. Li, J.B. Park, Y.K. Sun, F. Wu, K. Amine, Aprotic and Aqueous Li–O_2 Batteries, Chem. Rev. 114 (2014) 5611.
[17] H.D. Lim, H. Song, J. Kim, H. Gwon, Y. Bae, K.Y. Park, J. Hong, H. Kim, T. Kim, Y.H. Kim, X. Lepró, R. Ovalle-Robles, R.H. Baughman, K. Kang, Superior rechargeability and efficiency of lithium-oxygen batteries: hierarchical air electrode architecture combined with a soluble catalyst, Angew. Chem. Int. Ed. Engl. 126 (2014) 4007.
[18] Y. Inaguma, M. Nakashima, A rechargeable lithium–air battery using a lithium ion-conducting lanthanum lithium titanate ceramics as an electrolyte separator, J. Power Sources 228 (2013) 250.
[19] L.J. Li, A. Manthiram, Decoupled bifunctional air electrodes for high-performance hybrid lithium-air batteries, Nano Energy 9 (2014) 94.
[20] Z. Zhu, A. Kushima, Z.Y. Yin, L. Qi, K. Amine, J. Lu, J. Li, Anion-redox nanolithia cathodes for Li-ion batteries, Nature Energy 1 (2016) 16111.
[21] K. Hayashi, K. Shima, F. Sugiyama, A Mixed Aqueous/Aprotic Sodium/Air Cell Using a NASICON Ceramic Separator, J. Electrochem. Soc. 160 (2013) A1467.
[22] F. Liang, K. Hayashi, A High-Energy-Density Mixed-Aprotic-Aqueous Sodium-Air Cell with a Ceramic Separator and a Porous Carbon Electrode, J. Electrochem. Soc. 162 (2015) A1215.
[23] Y. Kang, F. Liang, K. Hayashi, Hybrid Sodium–Air Cell with Na[FSA–C_2C_1im][FSA] Ionic Liquid Electrolyte, Electrochimica Acta. 218 (2016) 119.
[24] H. Yadegari, Q. Sun, X. Sun, Sodium-Oxygen Batteries: A Comparative Review from Chemical and Electrochemical Fundamentals to Future Perspective, Adv. Mater. 28 (2016) 7065.
[25] H. Yadegari, M. Banis, A. Lushington, Q. Sun, R. Li, T.-K. Sham, X. Sun, A Bifunctional Solid State Catalyst with Enhanced Cycling Stability for Na and Li-O_2 Cells: Revealing the Role of Solid State Catalysts, Energy Environ. Sci. 10 (2017) 286.
[26] W. Yin, Z. Shadike, Y. Yang, F. Ding, L. Sang, H. Li, Z. Fu, A long-life Na–air battery based on a soluble NaI catalyst, Chem. Commun 51 (2015) 2324.
[27] T. Hashimoto, K. Hayashi, Aqueous and Nonaqueous Sodium-Air Cells with Nanoporous Gold Cathode, Electrochim. Acta 182 (2015) 809.

[28] W.M. Liu, W.W. Yin, F. Ding, L. Sang, Z.W. Fu, $NiCo_2O_4$ nanosheets supported on Ni foam for rechargeable nonaqueous sodium–air batteries, Electrochem. Commun. 45 (2014) 87.
[29] R.B. Araujo, S. Chakraborty, R. Ahuja, Unveiling the charge migration mechanism in Na_2O_2: implications for sodium-air batteries, Phys Chem Chem Phys 17 (2015) 8203.
[30] H. Yadegari, M.N. Banis, B.W. Xiao, Q. Sun, X. Li, A. Lushington, B.Q. Wang, R.Y. Li, T.K. Sham, X.Y. Cui, X.L. Sun, Three-Dimensional Nanostructured Air Electrode for Sodium–Oxygen Batteries: A Mechanism Study toward the Cyclability of the Cell, Chem. Mater. 27 (2015) 3040.
[31] S. Sahgong, S.T. SenthilKumar, K. Kim, S.M. Hwang, Y. Kim, Rechargeable Aqueous Na-Air Batteries: Highly Improved Voltage Efficiency by Use of Catalysts, Electrochem. Commun. 61 (2015) 53.
[32] B. Senthilkumar, Z. Khan, S. Park, I. Seo, H. Ko, Y. Kim, Exploration of cobalt phosphate as a potential catalyst for rechargeable aqueous sodium-air battery, J. Power Sources 311 (2016) 29.
[33] W. Liu, Q. Sun, Y. Yang, J.Y. Xie, Z.W. Fu, An enhanced electrochemical performance of a sodium–air battery with graphene nanosheets as air electrode catalysts, Chem. Commun 49 (2013) 1951.
[34] Z. Jian, Y. Chen, F. Li, T. Zhang, C. Liu, H. Zhou, High capacity Na-O_2 batteries with carbon nanotube paper as binder-free air cathode, J. Power Sources 251 (2014) 466.
[35] Y.L. Li, H. Yadegari, X.F. Li, M.N. Banis, R.Y. Li, X.L. Sun, Superior catalytic activity of nitrogen-doped graphene cathodes for high energy capacity sodium–air batteries, Chem. Commun. 49 (2013) 11731.
[36] Q. Sun, H. Yadegari, M.N. Banis, J. Liu, B.W. Xiao, B.Q. Wang, S. Lawes, X. Li, R.Y. Li, X.L. Sun, Self-stacked nitrogen-doped carbon nanotubes as long-life air electrode for sodium-air batteries: Elucidating the evolution of discharge product morphology, Nano Energy 12 (2015) 698.
[37] J.Y. Cheon, K. Kim, Y.J. Sa, S.H. Sahgong, Y. Hong, J. Woo, S.D. Yim, H.Y. Jeong, Y. Kim, S.H. Joo, Graghitic Nanoshell/Mesoporous Carbon Nanohybrids as Highly Efficient and Stable Bifunctional Oxygen Electrocatalysts for Rechargeable Aqueous Na-Air Batteries, Adv. Energy Mater. (2016) 1501794.
[38] X.M. Ge, Y.Y. Liu, F.W. Thomas Goh, T.S. Andy Hor, Y. Zong, P. Xiao, Z. Zhang, S.H. Lim, B. Li, X. Wang, Z.L. Liu, Dual-Phase Spinel $MnCo_2O_4$ and Spinel $MnCo_2O_4$/Nanocarbon Hybrids for Electrocatalytic Oxygen Reduction and Evolution, ACS Appl. Mater. Interfaces 6 (2014) 12684.
[39] L. Wang, F.X. Yin, C.X. Yao, N-doped graphene as a bifuctional electrocatalyst for oxygen reduction and oxygen evolution reactions in an alkaline electrolyte, J. Hydrogen. Energy 39 (2014) 15913.
[40] Z. Xiong, S.J. Liao, D. Dang, X.L. Tian, S.Y. Hou, F.F. Liu, H.L. Peng, Z.Y. Fu, Enhanced water management in the cathode of an air-breathing PEMFC using a dual catalyst layer and optimizing the gas diffusion and microporous layer, J. Hydrogen Energy 40 (2015) 3961.
[41] J. Li, S. Xiong, X. Li, Y. Qian, A Facile Route to Synthesize Multiporous $MnCo_2O_4$ and $CoMn_2O_4$ Spinel Quasi-Hollow Spheres with Improved Lithium Storage Properties, Nanoscale 5 (2013) 2045.
[42] L. Zhou, D. Zhao, X.W. Lou, Double-Shelled $CoMn_2O_4$ Hollow Microcubes as High-Capacity Anodes for Lithium-Ion Batteries, Adv. Mater. 24 (2012) 745.
[43] C. Li, X.P. Han, F.Y. Cheng, Y.X. Hu, C.C. Chen, J. Chen, Phase and composition controllable synthesis of cobalt manganese spinel nanoparticles towards efficient oxygen electrocatalysis, Nat. Commun. 6 (2015) 7345.
[44] D.J. Chen, C. Chen, Z.M. Baiyee, Z.P. Shao, F. Ciucci, Nonstoichiometric Oxides as Low-Cost and Highly-Efficient Oxygen Reduction/Evolution Catalysts for Low-Temperature Electrochemical Devices, Chem. Rev. 115 (2015) 9869.
[45] L.J. Li, A. Manthiram, O- and N-Doped Carbon Nanowebs as Metal-Free Catalysts for Hybrid Li-Air batteries, Adv. Energy Mater. 4 (2014) 1301795.
[46] L.J. Li, S.Y. Liu, A. Manthiram, Co_3O_4 nanocrystals coupled with O- and N-doped carbon nanoweb as a synergistic catalyst for hybrid Li-air batteries, Nano Energy 12 (2015) 852.
[47] L.J. Li, A. Manthiram, Decoupled bifunctinal air electrodes for high-performance hybrid lithium-air batteries, Nano Energy 9 (2014) 94.
[48] Z. Khan, B. SenthilKumar, S.O. Park, S. Park, J. Yang, J.H. Lee, H. Song, Y. Kim, S.K. Kwak, H. Ko, Carambola Shaped VO_2 Nanostructures: A Binder–Free Air Electrode for Aqueous Na–Air Battery J, Mater. Chem. A 5 (2017) 2037.